Synthesis, Characterization, and Morphogenesis of Carbonated Fluorapatite−Gelatine Nanocomposites: A Complex Biomimetic Approach toward the Mineralization of Hard Tissues

Elena V. Rosseeva, Jana Buder, Paul Simon, Ulrich Schwarz, Olga V. Frank-Kamenetskaya, and Rüdiger Kniep*

Max-Planck-Institut für Chemische Physik fester Stoffe, Nöthnitzer Strasse 40, 01187 Dresden, Germany, and Department of Crystallography, Saint Petersburg State University, Universitetskaya Nab 7/9, 199034 Saint Petersburg, Russia

Received February 27, 2008. Revised Manuscript Received July 16, 2008

Carbonated fluorapatite−gelatine nanocomposites were grown by the double-diffusion technique within a gelatine gel. The carbonate content was varied, whereas all other experimental parameters (Ca^{2+}, $[PO_4]^{3-}$, F^- concentrations, gel concentration, pH, temperature, and growth time) were kept constant. The composite aggregates grown within so-called Liesegang bands were characterized by XRD, chemical analysis, FT-IR and Raman spectroscopy, TG/DTA/MS, SEM and TEM. In the carbonated fluorapatite-gelatine nanocomposites the carbonate ions replace the phosphate groups (so-called B-type substitution). Apart from the fact that the biomimetic nanocomposites contain carbonated *fluor*apatite as the inorganic component, the chemical composition of the aggregates is similar to that of biological hard tissues. The content of carbonate, sodium, and the organic component in the biomimetic composites is closest to that of dental enamel. The morphogenesis of the carbonated composites was investigated as a function of the carbonate concentration in the solutions (also reflected in the carbonate content of the composites). In general, the morphogenesis of the carbonated composite aggregates is closely related to that of pure fluorapatite-gelatine nanocomposites (form development from a seed via dumbbell states to a notched sphere). With increasing carbonate content, however, the aggregates become significantly rounded and compressed, an observation that clearly reflects the decreasing coherence length ([001] direction) of the nanosubunits assembling the composite structure.

Introduction

Biological mineralization is an essential process in living organisms. It can be a normal phenomenon such as the formation of bone and teeth or a pathological process such as the formation of renal, dental, salivary, and other stones.[1−5] However, the process of biomineralization is very complex and specific for each hard tissue. The mineralization of bone and dentine occur under control of an organic matrix, which contains mostly collagenic protein (about 90 wt %). In contrast, the main components of the enamel extracellular matrix are noncollagenic proteins (amelogenins and enamelins).[2,6] Besides the structural insoluble organic matrix that provides a scaffold for the mineralization, the functional soluble organic matrix (such as amino acids, lipids, glycoproteins, etc.) also play an important role during the crystallization processes. Water-soluble organic macromolecules usually act as crystal modifiers and control the shape and architecture of crystallizing and growing inorganic materials. In biosystems, the hierarchical and self-similar organization of nanocomposite structures is of prominent relevance. Within the apatite−protein (collagen) nanocomposite structures (bone and teeth), a close orientational relationship between the triple-helical collagen molecules (arranged in form of fibrils) and the apatite nanocrystals is present. It is assumed that apatite first nucleates in the gaps between neighboring protein molecules.[7,8]

Biological apatite can generally be characterized as nonstoichiometric carbonated hydroxyapatite with a content of carbonate ions of about 1−9 wt %.[1,2,4,5] The role of carbonate ions during biological mineralization of hard tissues is not clearly understood up to now. However, it is well-known that the presence of carbonate in the apatite component usually increases its reactivity and dissolution behavior, conditions which are most important for the processes of re- and demineralization of biological hard tissues (bone and teeth).[1−3,9] It is generally accepted that

* Corresponding author. Tel.: 49-351-46 46 30 00. Fax: 49-351-46 46 30 02. E-mail: kniep@cpfs.mpg.de.

(1) Elliott, J. C.: *Structure and Chemistry of the Apatites and Other Calcium Orthophosphates*; Elsevier: Amsterdam, 1994.
(2) Elliott, J. C. *Rev. Miner. Geochem.* **2002**, *48*, 427.
(3) Dorozhkin, S. V. *J. Mater. Sci.* **2007**, *42*, 1061.
(4) Gross, K. A.; Berndt, C. C. *Rev. Miner. Geochem.* **2002**, *48*, 631.
(5) Frank-Kamenetskaya, O. V.; Golubtsov, V. V.; Pikhur, O. L.; Zorina, M. L.; Plotkina, Yu. V. *Proc. Russ. Mineral. Soc. (Zapiski RMO)* **2004**, *5*, 104.
(6) Golberg, M.; Septier, D.; Lecolle, S.; Chardin, H.; Quintana, M. A.; Acevedo, A. C.; Gafni, G.; Dillouya, D.; Vermelin, L.; Thonemann, B.; Schmalz, G.; Bissilamapahou, P.; Carreau, J. P. *Int. J. Dev. Biol.* **1995**, *39*, 93.
(7) Heywood, B. R.; Sparks, N. H. C.; Shellis, R. P.; Weiner, S.; Mann, S. *Connect. Tissue Res.* **1990**, *25*, 103.
(8) Landis, W. J.; Hodgens, K. J.; Arena, J.; Song, M. J.; McEwen, B. F. *Microsc. Res. Techn.* **1996**, *33*, 192.
(9) Shimoda, S.; Aoba, T.; Moreno, E. C.; Miake, Y. *J. Dent. Res.* **1990**, *69*, 1731.

10.1021/cm8005748 CCC: $40.75
Published on Web 09/17/2008

carbonate ions can substitute for both OH^-(F^-) ions in the channels running along [001] of the apatite crystal structure (so-called A-type substitution) and the phosphate groups (so-called B-type substitution), respectively.[1,10−14] In case of the B-type substitution, the lattice parameter *a* decreases while *c* slightly increases with the carbonate content, whereas the A-type substitution results in a progressive increase of the *a* parameter.[1,2,10−14] Previous investigations demonstrated that biological apatite contains B- and A-type carbonate ions in its crystal structure; however, the B-type substitution is most common.[1,3,5,11] Recent results also showed that the content of carbonate (mainly B-type substitution) as well as fluoride in the apatite component of enamel increases with increasing age of the biomaterial.[3,5]

The growth of model systems such as inorganic−organic hybrid materials under controlled mineralization conditions is important for a deeper understanding of the mechanisms of biomineralization. Our previous investigations were devoted to the biomimetic growth of fluorapatite−gelatine nanocomposites.[15−24] The present work is a further step toward mimicking natural composite systems by focusing on the biomimetic synthesis of carbonated fluorapatite−gelatine nanocomposites. This system is more complex and significantly closer related to the respective biosystem, which plays a decisive role in the process of biological mineralization of hard tissues.

Experimental Section

Composite Growth. The biomineralization process was mimicked by a double-diffusion arrangement. The carbonated fluorapatite−gelatine nanocomposites were grown according to slightly modified procedures reported previously for fluorapatite−gelatine nanocomposites.[15−18] The growth of the composites was carried out in U-tubes according to the double diffusion technique in which reservoirs of two reagent solutions are separated by a gelatine gel plug [pig-skin gelatine (300 bloom, Aldrich), concentration 10 wt %]. The gel plug was approximately 5 cm in length and 120 cm^3 in volume. The L-shaped tubes of the diffusion cells were filled with buffered aqueous solutions of $CaCl_2$ (0.1333M) and Na_2HPO_4/Na_2CO_3/NaF, respectively. Na_2CO_3 was added to the phosphate solution in order to obtain molar ratios Ca:P:C:F of 5:5:*x*:1, with variation of *x* in steps of 0.5 or 1 between 0 and 9. Tris-(hydroxymethyl)-methylamine was used to buffer the solutions and the starting pH was adjusted to 7.40(2) using 2 M HCl. The pH value of the gelatine was set to 3.0(2) in order to get a low supersaturation in the initial stage of phase crystallization and to prevent the formation of $CaCO_3$ and CaF_2. In the first stage of the growth reaction, the release of CO_2 was observed; however, after some days, the pH of gelatine increased up to 6−7, thus stabilizing the HCO_3^- and CO_3^{2-} species. The temperature was held constant during the experiments at 25 °C using a water bath. Within periods of 3 weeks, so-called Liesegang bands were formed containing the composite aggregates. Those Liesegang bands, which are located close to the calcium and phosphate sources, are named C and P, respectively. The M bands (middle bands) are located between P and C [15−24] (Figure 1). To isolate the aggregates from the gel, the gelatine plug was pressed out of the tube and cut into slices consisting of the different Liesegang bands. The isolated Liesegang segments were treated with water and the products were washed five times in distilled water at 40 °C, centrifuged and finally dried at 40 °C.

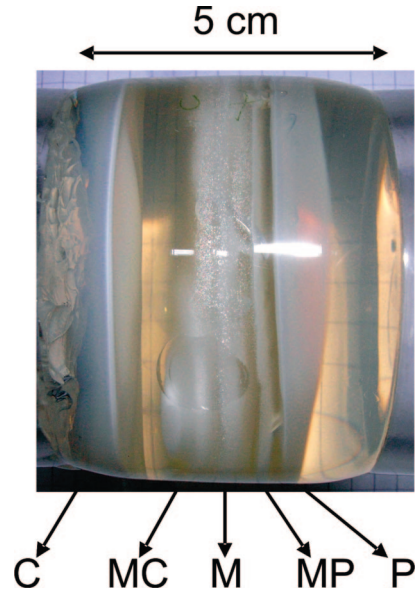

Figure 1. Periodic growth of carbonated fluorapatite−gelatine composites (formation of Liesegang bands) within a gelatine gel by use of the double diffusion technique. The bands are described as C, M, and P, respectively, showing their positions in the diffusion tube (C = bands close to the calcium source, M = middle bands, P = bands close to the phosphate (carbonate, fluoride source).

Characterization. *X-Ray Diffraction.* The phase composition of the aggregates was determined by X-ray diffraction analyses. X-ray powder data were collected in transmission mode using a Huber G670 Image Plate Camera, Cu Kα1 radiation (λ = 1.540598 Å) and germanium (111) monochromator. Lattice constants *a* and *c* of apatite were calculated by least-squares refinements using LaB_6 (cubic, *a* = 4.15692 Å) as internal standard and the program package WinCSD.[25] The coherence length of the carbonated fluorapatite domains along their *c*- and *a*-axes was calculated from the Scherrer equation using the (002) and (100) reflections, respectively, and an abiogen fluorapatite as a standard.

FT-IR Spectroscopy. Fourier transform infrared (FT-IR) spectra in the region of 4000−400 cm^{-1} were recorded at room temperature using a Bruker spectrometer (IFS 66v/S; Globar (MIR), KBr, DTGS-Detector; Program Opus/IR 3.0.3). The samples were prepared as KBr pellets (1 mg of the material under investigation

(10) LeGeros, R. Z. Crystallography Studies of the Carbonate Substitution in the Apatite Structure. PhD thesis, New York University, New York, 1967.
(11) Wilson, R. M.; Elliott, J. C.; Dowker, S. E. P. *Am. Mineral.* **1999**, *84*, 1406.
(12) Wilson, R. M.; Elliott, J. C.; Dowker, S. E. P.; Smith, R. I. *Biomaterials* **2004**, *25*, 2205.
(13) Fleet, M. E.; Liu, X. *Biomaterials* **2007**, *28*, 916.
(14) Ivanova, T. I.; Frank-Kamenetskaya, O. V.; Kol'tsov, A. B.; Ugolkov, V. L. *J. Solid State Chem.* **2001**, *160*, 340.
(15) Kniep, R.; Busch, S. *Angew. Chem.* **1996**, *108*, 2787. *Angew. Chem., Int. Ed.* **1996**, *35*, 2624.
(16) Busch, S.; Dolhaine, H.; DuChesne, A.; Heinz, S.; Hochrein, O.; Laeri, F.; Podebrand, O.; Vietze, U.; Weiland, T.; Kniep, R. *Eur. J. Inorg. Chem.* **1999**, *10*, 1643.
(17) Busch, S.; Schwarz, U.; Kniep, R. *Adv. Funct. Mater.* **2003**, *13*, 189.
(18) Busch, S.; Schwarz, U.; Kniep, R. *Chem. Mater.* **2001**, *13*, 3260.
(19) Simon, P.; Zahn, D.; Lichte, H.; Kniep, R. *Angew. Chem.* **2006**, *118*, 1945. *Angew. Chem., Int. Ed.* **2006**, *45*, 1911.
(20) Simon, P.; W.; Carrillo-Cabrera, W.; Formanek, P.; Göbel, C.; Geiger, D.; Ramlau, R.; Tlatlik, H.; Buder, J.; Kniep, R. *J. Mater. Chem.* **2004**, *14*, 2218.
(21) Simon, P.; Schwarz, U.; Kniep, R. *J. Mater. Chem.* **2005**, *15*, 4992.
(22) Tlatlik, H.; Simon, P.; Kawska, A.; Zahn, D.; Kniep, R. *Angew. Chem.* **2006**, *118*, 1939. *Angew. Chem., Int. Ed.* **2006**, *45*, 1905.
(23) Kniep, R.; Simon, P. *Top. Curr. Chem.* **2007**, *270*, 73.
(24) Kniep, R.; Simon, P. *Angew. Chem., Int. Ed.* **2008**, *47*, 405.

dispersed in 150 mg KBr). In order to separate the overlapping bands the spectral ranges were fitted with Pseudo-Voigt 1 distributions for the bands. The software package Origin 7.0 (OriginLab Corporation, MA, USA) was used for the calculations.

Raman Spectroscopy. Raman spectra in the region of 1500−300 cm^{-1} were collected at room temperature using a LabRam System 010 (Horiba Jobin Yvon, France) in backscattering mode. The 632.817 nm line of a He−Ne laser with 1 mW light power was used for excitation of samples under a microscope (20× magnification). For the sample measurements, ground powder was spread on a glass plate. The spectra were collected within two hours or overnight. The spectrometer was calibrated using Si as a reference. In order to separate the overlapping bands the spectral ranges were fitted with Pseudo-Voigt 1 distributions for the bands. The software package Origin 7.0 (OriginLab Corporation, MA, USA) was used for the least-squares fits.

Chemical Analyses. To prepare the samples for chemical analysis, we ground the composite aggregates isolated from the M-Liesegang bands and then washed them 3 times for 20 min in distilled water at 40 °C; they were then centrifuged and finally dried at 40 °C. These procedures were used to remove the fraction of gelatine, which is not tightly embedded in the inorganic component of the aggregates.

The content of calcium, phosphate, and sodium was determined by inductively coupled plasma-optical emission spectrometry (ICP-OES, Varian, VISTA RL). For the measurements, 10 mg samples were dissolved in 4 mL of 2 M HCl and then diluted with water in a 100 mL volumetric flask. The fluoride content was determined by using F-ion-selective electrode (Mettler Toledo Inc., Wilmington, MA). The amounts of carbonate and gelatine were calculated on the basis of the C and N contents determined by use of the carrier-gas hot-extraction method combined with the combustion technique by means of the CHNS-analyzer 932 (LECO, USA). The sample weights amounted to 2 mg and combustion was performed in Sn capsules under an O_2 atmosphere.

TG/DTA/MS. The decomposition processes of carbonated fluorapatite-gelatine-nanocomposites were investigated by means of a Netzsch thermal analyzer STA 409, coupled with a capillary mass spectrometer QMS 403C-Aeolos. The sample weights were 30 mg and heating was performed in a corundum crucible with a rate of 10 K/min up to 1200 °C in air.

Scanning and Transmission Electron Microscopy. The morphology and inner structure of the synthetic aggregates were studied by scanning electron microscopy (SEM) and transmission electron microscopy (TEM). SEM investigations were performed by means of an ESEM FEI Quanta 200 FEGi system operated in a low vacuum (60 Pa) mode and at an acceleration voltage of 15 kV (FEI Company, Eindhoven, The Netherlands). For TEM investigations focused ion beam (FIB) thin cuts of the aggregates were prepared by means of a FEI Quanta 200 3D dual beam device (FEI Company). For this purpose the samples were deposited from an ethanol suspension onto a thin silicon wafer bar. Microtome specimens were prepared by embedding the composite particles in epoxy resin and cutting ~70 nm slices by using a Ultracut UCT ultramicrotome (Leica company, Wetzlar, Germany). TEM experiments were carried out by using a FEI Tecnai 10 electron microscope (FEI Company) with LaB_6 source at 100 kV acceleration voltage. Images were recorded with a Tietz slow scan CCD F224HD TVIPS camera (2k × 2k pixels, pixel size 24 μm, digitization 16 bit) with an active area of 49 mm × 49 mm. (Tietz Video and Image Processing Systems GmbH, Gauting, Germany).

Statistics. Statistical data analyses were performed by use of the Statistica 6.0 software package (StatSoft, Inc., Tulsa, OK).

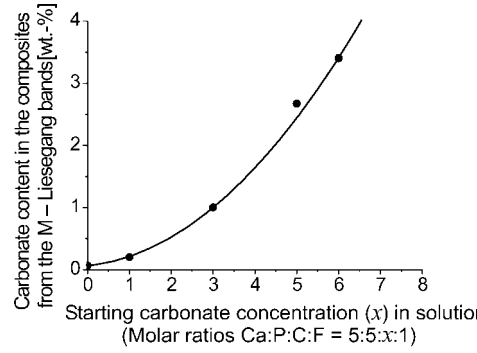

Figure 2. Carbonate content in the composites isolated from the M-Liesegang bands in the gelatine gel as a function of the concentration of carbonate ions (molar ratio Ca:P:C:F = 5:5:*x*:1) in the starting solutions (the initial pH of the gelatine gel was adjusted to 3.05(5)). The nonlinear regression curve indicates the multifactor character of the growth process of carbonated fluorapatites aggregates. Error bars that indicate statistical error of the chemical analysis are smaller than the size of the symbols (black dots). For further details, see the text.

Results and Discussion

Chemical Composition. The biomimetically grown aggregates can be characterized as inorganic−organic composites consisting of gelatine (organic component) and carbonated fluorapatite (inorganic component). The N and C contents of pure gelatine (educt) were determined experimentally and correspond to 17.0(1) and 45.3(1) wt %, respectively. Thus, the amount of gelatine [Gelatine] in the aggregates was determined on the basis of the N content [N] and calculated as follows: [Gelatine](wt %) = [N]5.88, which corresponds to about 2−3 wt %.

The content of carbonate ions ($C_{CO_3^{2-}}$) was calculated on the basis of the difference between the total C content [C] in the aggregates and C content corresponding to the gelatine component according to the following equation: $C_{CO_3^{2-}}$(wt %) = 5([C] − [N]2.67). The chemical composition of the composite aggregates strongly depends on the growth conditions. Figure 2 illustrates the relationship between the carbonate content in the composites (isolated from the M Liesegang bands) and the initial molar ratio (*x*) of the carbonate ions in solution (the initial pH of the gelatine gel was 3.05(5)). The carbonate content in the composites increases with the increase of carbonate concentration in the starting solutions. Thus, the composition of apatite in the aggregates strongly differs from stoichiometric fluorapatite. Besides the "built-in" carbonate and sodium ions, we also determined a Ca deficiency and a deficiency of $F^-(OH^-)$ ions, resulting in a variable Ca:P molar ratio of the apatite component. Figure 3A shows the relationship between the $[CO_3]^{2-}$ content and the Ca:P molar ratio of carbonated fluorapatite in the composites on the basis of the results of chemical analyses. The gradual increase of the Ca:P molar ratio with increasing carbonate content in the composites is compatible with a substitution of phosphate groups by carbonate ions in the fluorapatite crystal structure.[1,10] This so-called B-type substitution is suggested by our results of the vibration spectroscopy and XRD investigations (see below). According to literature data,[11,26−27] the process of substitution of $[PO_4]^{3-}$ by $[CO_3]^{2-}$ usually causes the formation of vacancies on the calcium site as well as within

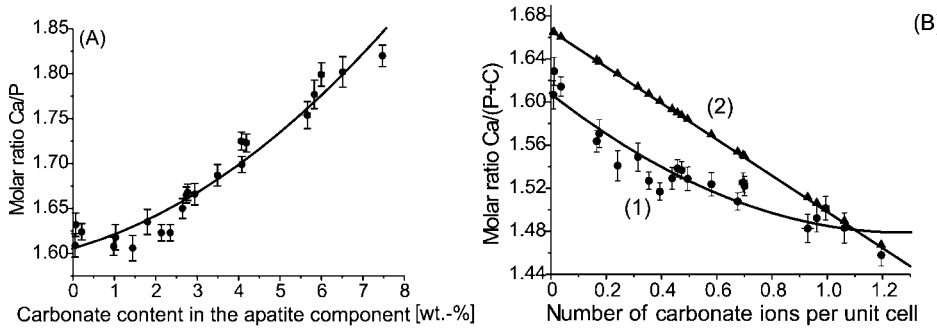

Figure 3. (A) Variation in the molar ratio Ca:P of the carbonated fluorapatite composites with varying content of carbonate. (B) Variation in the Ca:(P+C) molar ratio (C = carbonate carbon) of the carbonated fluorapatite composites with different carbonate contents: (1) experimental data; (2) theoretical calculation corresponding to substitution scheme I for the isomorphic substitution of phosphate by carbonate. For a discussion of the discrepancy, see the text. Error bars are shown as vertical and horizontal lines if larger than the size of symbol (black dots).

the channels of the apatite crystal structure according to the following scheme of substitution

$$Ca^{2+} + [PO_4]^{3-} + F^-(OH^-) \leftrightarrow \square_{Ca} + [CO_3]^{2-} + (\square_{F^-(OH^-)}; H_2O) \quad (I)$$

Figure 3 (B) illustrates the relationship between the $[CO_3]^{2-}$ content and the molar ratio Ca/(P+C) of apatite on the basis of the experimental data (1) as well as from theoretical calculations (2) corresponding to substitution scheme I. The Ca/(P+C) ratio decreases with increasing $[CO_3]^{2-}$ content. However, for a given carbonate content the experimental points indicate a calcium deficiency higher than that corresponding to substitution scheme I. First of all this means that part of Ca^{2+} is substituted by Na^+ (scheme II). Additionally formation of vacancies on the Ca^{2+}sites can be realized by substitution scheme III causing partial substitution of $[PO_4]^{3-}$ by $[HPO_4]^{2-}$ ions.[9,26−30] The existence of $[HPO_4]^{2-}$ ions in the apatite component was also confirmed by vibration spectroscopy investigations (see below).

$$Ca^{2+} + [PO_4]^{3-} \leftrightarrow Na^+ + [CO_3]^{2-} \quad (II)$$

$$Ca^{2+} + [PO_4]^{3-} + F^-(OH^-) \leftrightarrow \square_{Ca} + [HPO_4]^{2-} + (\square_{F^-(OH^-)}; H_2O) \quad (III)$$

Thus, the development of a general apatite formula is based on the assumption, that the phosphate sites in the apatite crystal structure are fully occupied by the sum of $[PO_4]^{3-}$, $[HPO_4]^{2-}$ and $[CO_3]^{2-}$ groups. The total content of these anions is set to six (per stoichiometric apatite formula $Ca_{10}(PO_4)_6F_2$); Na^+ is assigned to the Ca^{2+} site. Charge balance is maintained by replacement of parts of the $[PO_4]^{3-}$ groups with $[HPO_4]^{2-}$ ions and also by formation of vacancies in, both, the Ca^{2+} and F^- sites to give a charge-balanced formula according to the substitution schemes I−III.

Table 1. Chemical Composition of the Inorganic Fraction and Content of the Organic Component of Natural Human Hard Tissues[2−5] and the Biomimetic Composite Isolated from the M-Liesegang Bands (wt %)

element	carbonated fluorapatite gelatine composite	enamel	dentine	bone
Ca	35.4–37.1	33.9–39.3	34.9–40.4	36.6–37.7
Na	0.5–1.1	0.5–1.0	0.9–1.4	0.8–1.0
Mg		0.2–0.3	0.8–1.0	0.6–1.1
P	15.5–17.9	16.1–18.8	16.9–19.5	17.1–17.7
$[CO_3]^{2-}$	0.05–7.5	1.6–7.8	1.0–6.5	6.5–8.9
F	3.1–4.2	0.1–0.3	0.07	0.03–0.1
Cl		0.3–0.4	0.03–0.27	0.1–0.2
organic component	2–3	1–4	20–30	25–40

Thus, the general empirical formula for carbonated fluorapatite in the composites (from the M Liesegang bands) is given as follows based on the experimental analytical data of content Ca, Na, P, C, and F (Table 1):

$$(Ca_xNa_y\square_{10-(x+y)})\{[PO_4]_{n-z}[CO_3]_k[HPO_4]_z\} \times \{F_m[OH]_s,(\square,H_2O)_{2-(s+m)}\} \quad (1)$$

where $x = 8.75-9.77$; $y = 0.24-0.49$; $n = 4.80-5.99$; $k = 0.01-1.20$; $z = 0.99-0.22$; $m = 2-1.73$; $s < 0.2$; $(x + y) \leq 10$; $(m + s) \leq 2$; $(n + k) = 6$; $z = (12 + n + s + m - 2x - y)$.

Table 1 shows the results of the chemical analyses of the biomimetic carbonated fluorapatite−gelatine nanocomposites (from the M Liesegang bands) compared with the chemical composition of human dental enamel, dentine and bone, respectively.[1−5] As mentioned already earlier, the inorganic component of these human hard tissues can be characterized as nonstoichiometric carbonated hydroxyapatite. Thus, apart from the fact that the biomimetic apatite−gelatine nanocomposites under consideration contain carbonated *fluor*apatite as the inorganic component, the chemical composition of the aggregates is similar to that of biological hard tissues. The content of carbonate, sodium, and the organic component is closest to that of dental enamel.

X-Ray Diffraction. X-Ray diffraction analyses showed that the composites grown with initial molar ratios (x) of carbonate ions in solution from 0 to 8, gave well-resolved apatite pattens. Reflections corresponding to those of calcium

(25) Akselrud, L. G.; Zavalii, P. Y.; Grin, Yu. N.; Pecharsky, V. K.; Baumgartner, B.; Wölfel, E. *Mater. Sci. Forum* **1993**, *133−136*, 335.
(26) Pieters, I. Y.; De Maeyer, E. A. P.; Verbeeck, R. M. H. *Inorg. Chem.* **1998**, *37*, 6392.
(27) De Maeyer, E. A. P.; Verbeeck, R. M. H.; Naessens, D. E. *Inorg. Chem.* **1993**, *32*, 5709.
(28) Mantel, G.; Bonel, G.; Heughebaert, J. C.; Trombe, J. C.; Rey, C. *J. Cryst. Growth* **1981**, *53*, 74.
(29) LeGeros, R. Z.; Trautz, O. R.; LeGeros, J. P.; Klein, E. *Bull. Soc. Chim. Fr.* **1968**, Special No. 1712.
(30) Panova, E. G.; Ivanova, T. I.; Frank-Kamenetskaya, O. V.; Bulach, A. G.; Chukanov, N. V. *Proc. Russ. Mineral. Soc. (Zapiski RMO)* **2001**, *4*, 97.

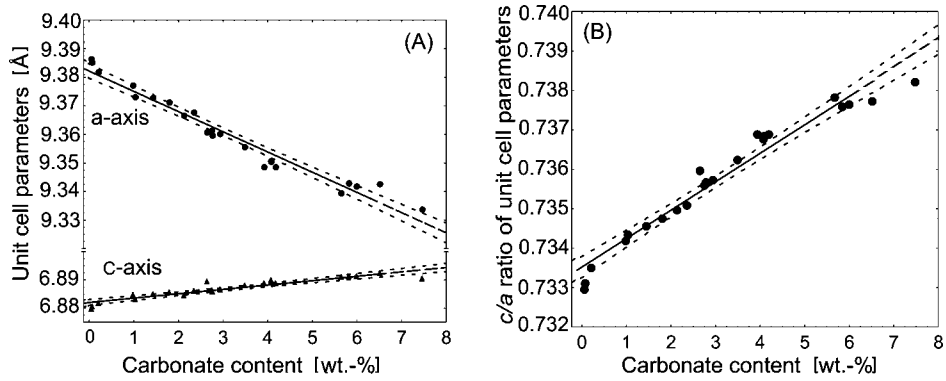

Figure 4. Variation of the lattice parameters of biomimetic carbonated fluorapatite with different carbonate contents. (A) Lattice parameters *a* and *c* of apatite; (B) *c*/*a* ratio of apatite. The dashed lines indicate the 95% confidence interval for the regression lines.

carbonate polymorphs, calcium fluoride or other calcium phosphates were not observed. Calcium carbonate (calcite) was only identified in the C Liesegang band in an experiment with relatively high carbonate concentration of $x \approx 9$ in the initial solution. The results of the determination of the lattice parameters of the biomimetic apatites showed that with increasing content of carbonate, the lattice parameter *a* decreased, whereas the parameter *c* slightly increased (Figure 4A). In addition, the *c*/*a* ratio increased with increasing carbonate content of the apatite component (Figure 4B). This finding is confirmed by the regression analysis for 23 data points, which shows that the correlation between these parameters is linear at the 95% significance level and is given by the equations

$$a\ (\text{Å}) = (9.3822 \pm 0.0025) - (7.1 \pm 0.7) \times 10^{-3}(CO_3^{2-}\text{content/wt \%}),\ [SE = 0.0032;\ R = 0.979] \quad (2)$$

$$c\ (\text{Å}) = (6.8820 \pm 0.0011) + (1.6 \pm 0.3) \times 10^{-3}(CO_3^{2-}\text{content/wt \%}),\ [SE = 0.00133;\ R = 0.930] \quad (3)$$

$$c/a = (7.3352 \pm 0.0027) \times 10^{-1} + (7.2 \pm 0.7) \times 10^{-4}(CO_3^{2-}\text{content/wt \%}),\ [SE = 0.00034;\ R = 0.977] \quad (4)$$

where SE is the standard error of estimate and *R* is the coefficient of correlation.

The variation in the lattice constant with the carbonate content also agrees with the values calculated from the data of LeGeros (8 data points) for carbonated fluorapatite.[10] In accordance with literature data, the observed relationships between the carbonate content and variations of the lattice parameters of apatite are typical for so-called B-type carbonated apatite (phosphate replacement).[10,12,13,29] B-type substitution of carbonate ions in the biomimetic composites is also corroborated by the vibration spectroscopy investigations (see below).

Furthermore, it was established that the *c*/*a* ratio and the carbonate content in the fluorapatite-gelatine-nanocomposites isolated from different Liesegang bands increases from the P to the C side (Figure 5). This tendency was confirmed in all experiments with an initial molar ratio *x* of carbonate greater than zero in the solutions. This finding suggests that increasing incorporation of carbonate ions into the fluorapatite crystal structure may be due to an increasing ratio $[CO_3]^{2-}/[PO_4]^{3-}$ within the gelatine gel during the double diffusion process.

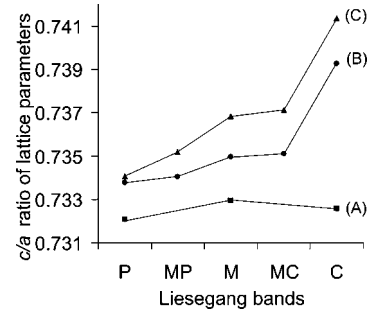

Figure 5. *c*/*a* ratios of the unit-cell parameters of carbonated fluorapatite from the biomimetic composites isolated from different Liesegang bands with different concentrations of carbonate ions (molar ratio Ca:P:C:F = 5:5:*x*:1) in the starting solutions (the initial pH of gelatine gel was 3.05(5)): (A) $x = 0$; (B) $x = 5$; (C) $x = 7.5$.

Vibration Spectroscopy. The presence of $[PO_4]^{3-}$, $[HPO_4]^{2-}$, $[OH]-$, $[CO_3]^{2-}$, H_2O, and protein molecules in the biomimetic composites was monitored by FTIR and Raman spectroscopy, which are powerful methods in studying ionic substitutions and have been widely used in synthetic and natural apatite research. However, the identification of IR- and Raman-bands in complex, substituted biological apatite composite material (bone, teeth, etc.) is a more difficult issue. In this case, synthetic samples with well-known chemical composition are used as model substances to investigate composite biological hard tissues. For crystal structures lacking inversion symmetry, the vibrational activity of modes is complementary in Raman and IR spectroscopy. Furthermore, the use of both spectroscopy techniques allows solving the problem of separation and identification of overlapping bands and determining the presence of structural specimens.

Figures 6 and 7 show the representative FT–IR and Raman spectra of carbonated fluorapatite-gelatine-nanocomposite obtained from the M-band with contents of carbonate and gelatine of 5.9 and 2.4 wt %, respectively. These spectra are similar to those of carbonated hydroxyapatite-protein composites and also to some biological hard tissues previously reported by several authors.[1,5,32] Both FT–IR and Raman spectra of the biomimetic composite exhibit four modes (ν_1, ν_2, ν_3, ν_4) attributed to the internal vibration of the phosphate group[1,31−36] (Table 2). In addition, the bands corresponding to the $[HPO_4]^{2-}$ group are detected in the Raman spectra at 874 and 1006 cm^{-1} (as distinguishable

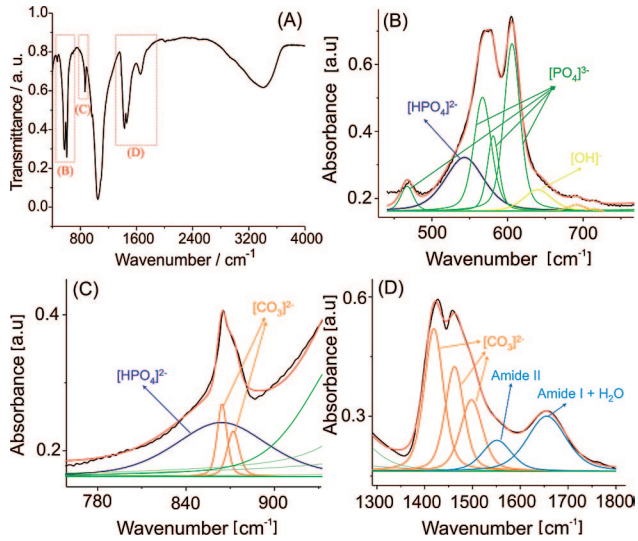

Figure 6. FT-IR spectrum of the biomimetic carbonated fluorapatite−gelatine composite with contents of carbonate and gelatine of 5.9 and 2.4 wt %, respectively. (A) Complete FT-IR spectrum from 4000 to 400 cm^{-1} (red dashed frames indicate the selected regions B, C, and D); (B−D) Selected regions of the FT-IR spectrum fitted with Pseudo-Voigt 1 distributions for the bands. Experimental data are indicated by black lines. The green, purple, orange, yellow, and blue lines show the individual bands corresponding to $[PO_4]^{3-}$, $[HPO_4]^{2-}$, $[CO_3]^{2-}$, $[OH]^-$, and amide groups, respectively. The red line is the resulting calculated spectrum. For further details, see the text.

peaks) (panels B and C in Figure 7)[35] as well as in the IR spectra at 545 and 864 cm^{-1} (as broad shoulders) (panels B and C in Figures 6).[31,34] The infrared absorption bands of carbonate were found at 865 cm^{-1} with a shoulder at 873 (ν_2) (Figure 6C), 1420 cm^{-1} (ν_3), and 1462 cm^{-1}, with a shoulder at 1498 (ν_3) cm^{-1} (Figure 6D) and weak bands at 692 and 715 cm^{-1} (ν_4) (Figure 6B), which correspond to the B-type carbonate substitution (phosphate replacement).[1,2,8,28,29] B-type substitution of carbonate ions is also confirmed by the Raman investigations showing the appearance of the characteristic band at 1070 cm^{-1} (Figure 7C). In addition, all the IR spectra display a band at 1546 cm^{-1}, which can be attributed to the A-type carbonate substitution (ν_3) as well as to amide II.[1,2,28,29,37] However, in the Raman spectra the band at 1107 cm^{-1}characteristic for an A-type carbonate substitution[35] was not observed. This finding allows us to exclude the presence of carbonate ions within the channels of the apatite crystal structure (A-type substitution) in the grown aggregates. Furthermore, in the biomimetic carbonated fluorapatite-gelatine-nanocomposites the IR peak ν_2 of the carbonate group (Figure 6C) is slightly shifted by ~5−7 cm^{-1} to a lower frequency with respect to carbonated hydroxyapatite.[33,38] This observation is typical for carbonated fluorapatites and can be explained by the significant influence of the fluoride ions on the conformation of carbonate ions in the apatite crystal structure.[38] The FT-IR spectra of all samples under investigation show a broadband in the high energy region from 3700 to 2700 cm^{-1} and a band at about 1650 cm^{-1} (overlap with the amide I band, see below) that can be assigned to the water molecule stretching and bending modes, respectively.[1,2] The bands located at 1655, 1546, and 1240 cm^{-1} were assigned to the absorption of amide I, amide II (Figure 6D), and amide III, respectively. The appearance of amide bands in these positions indicates that the proteins in the carbonated fluorapatite−gelatine nanocomposites have the α-helical configuration.[37] Additionally, amide A and B exhibit bands at 3070 − 3300 cm^{-1},[37] which overlap with the stretching modes of the water molecules. The vibration modes of the CH groups of the gelatine molecules were found at 2853, 2925, and 2960 cm^{-1}. In the Raman spectra the weak bands at 1002, 1245, and 1450 cm^{-1} are assigned to the phenyl, amide III and CH groups of gelatine molecules, respectively[35] (panels C and D in Figure 7). Trace amounts of $[OH]^-$ groups in the apatite component of the composite are indicated by the existence in the FT-IR-spectra of a broad weak band at 640 cm^{-1} and weak bands at 692 and 715 cm^{-1} (overlap with the ν_4 carbonate band) which can be assigned to OH^- librational modes.[39] The $[OH]^-$ stretching band (at 3540 cm^{-1}) was not observed.

Thermal Decomposition. The decomposition of the biomimetic composite with increasing temperature was investigated by TG/DTA/MS. The thermally induced changes in the carbonated fluorapatite-gelatine nanocomposites are very complex, involving overlapping reactions with the release of several gaseous species. It is not possible to resolve the reactions from the TG curves alone; additional information can be obtained from DTA and mass-spectroscopy (MS) which allow a correlation of the mass loss to specific degradation products and reactions. Figure 8 shows a representative DTA/TG/DTG and the respective MS diagram of the thermal decomposition of the composite with an initial content of carbonate and gelatine of 5.8 and 2.3 wt %, respectively. The data for the thermal decomposition clearly indicate a stepwise mass loss (Figure 8 A and Table 3). The first step beginning at room temperature is finished at 200 °C and is related to the release of adsorbed water from the aggregates. The endothermic peak in the DTA curve corresponding to the desorption of water appears at 100 °C. The second step (200−600 °C) is more complex and is characterized by the release of the main fragments with molecular masses of 18 and 44, corresponding to H_2O and CO_2, respectively (Figure 8B). Small amounts of fragments with molecular masses 12, 25, 42, 46, 51, 56 indicate the release of products of partial decomposition and simultaneous oxidation of gelatine (C^+, $C_3H_6^+$, $C_2H_5OH^+$, $NH^+{=}CH_2{-}R$ and others). The strong and broad exothermic peak at 340 °C (maximum) corresponds to the thermal degradation and pyrolysis of gelatine. According to literature data,[1,40] in this temperature range, the release of H_2O and CO_2 from the

(31) Wilson, R. M.; Elliott, J. C.; Dowker, S. E. P.; Rodriguez-Lorenzo, L. M. *Biomaterials* **2005**, *26*, 1317.
(32) Yang, Z. W.; Jiang, Y. S.; Yu, L. X.; Wen, B.; Li, F. F.; Suna, S. A. M.; Houa, T. Y. *J. Mater. Chem.* **2005**, *15*, 1807.
(33) Antonakos, A.; Liarokapis, E.; Leventouri, T. *Biomaterials* **2007**, *28*, 3043.
(34) Rey, C.; Shimizu, M.; Collins, B.; Glimcher, M. J. *Calcif. Tissue Int.* **1990**, *46*, 384.
(35) Penel, G.; Leroy, G.; Rey, C.; Bras, E. *Calcif. Tissue Int.* **1998**, *63*, 475.
(36) Awonusi, A.; Morris, M. D.; Tecklenburg, M. M. J. *Calcif. Tissue Int.* **2007**, *81*, 46.
(37) Doyle, B. B.; Bendit, E. G.; Blout, E. R. *Biopolymers.* **1975**, *14*, 937.
(38) Okazaki, M. *Calcif. Tissue Int.* **1983**, *35*, 78.
(39) Freund, F.; Knobel, R. M. *J. Chem. Soc., Dalton Trans.* **1977**, 1136.

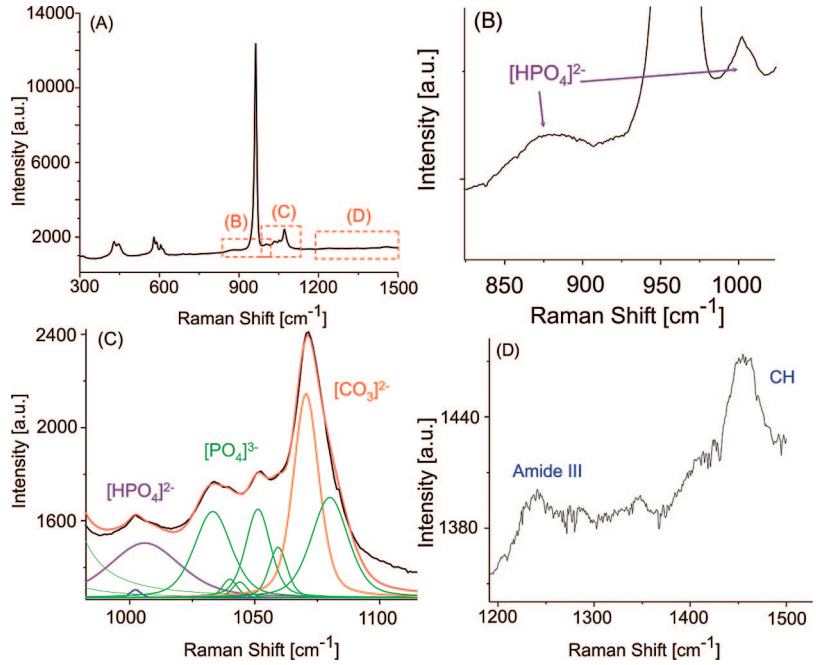

Figure 7. Raman spectrum of the biomimetic carbonated fluorapatite−gelatine composite with contents of carbonate and gelatine of 5.9 and 2.4 wt %, respectively. (A) Complete Raman spectrum from 1500 to 300 cm^{-1} (red dashed frames indicate the selected regions B, C, and D); (B, D) selected zoomed regions of the Raman spectra; (C) slected regions of the Raman spectra fitted with Pseudo-Voigt 1 line shapes for the bands. Experimental data are indicated by black lines. The green, purple, orange, and blue lines show the individual contributions corresponding to $[PO_4]^{3-}$, $[HPO_4]^{2-}$, $[CO_3]^{2-}$, and phenyl groups, respectively. The red line is the resulting calculated profile. For further details, see the text.

Table 2. IR and Raman Vibration Modes Observed for the Carbonated Fluorapatite Gelatine Composite and Their Assignments (OS, out of scale; NO, not observed)

vibration mode	IR (cm^{-1})	Raman (cm^{-1})
$[PO_4]^{3-}$ ν_1	964	962
$[PO_4]^{3-}$ ν_2	468	430
		445
$[PO_4]^{3-}$ ν_3	1032	1033
	1096	1040
	1155	1044
		1051
		1060
		1080
$[PO_4]^{3-}$ ν_4	567	579
	581	589
	606	605
		614
$[HPO_4]^{2-}$	545	874
	864	1006
B-type $[CO_3]^{2-}$ ν_1	NO	1070
B-type $[CO_3]^{2-}$ ν_2	865	NO
	873	
B-type $[CO_3]^{2-}$ ν_3	1420	NO
	1462	
	1498	
B-type $[CO_3]^{2-}$ ν_4	692	NO
	715	
$[OH]^-$	640	NO
	692	
	715	
H_2O	3700 − 2700	OS
amide I	1655	OS
amide II	1546	OS
amide III	1240	1245
amide A, B	3070 − 3300	OS
phenyl (phenylalanine)	NO	1002
CH	2853	1450
	2925	
	2960	

carbonated fluorapatite may be also caused by the reaction of $[HPO_4]^{2-}$ with $[CO_3]^{2-}$ as well as by transformation of $[HPO_4]^{2-}$ to $[P_2O_7]^{4-}$ by releasing H_2O molecules and also by release of constitutional water from the channels running along [001] of the apatite crystal structure. The third step starts around 600 °C and is associated with the final thermal decomposition of residual organics and the whole removal of carbonate ions from the carbonated fluorapatite composite. The MS investigation reveals that the release of CO_2 is completed at 900 °C (Figure 7B). This process is also indicated by the exothermic peak in the DTA curve at 740 °C (maximum). It was also shown that the lattice parameter *a* of fluorapatite after thermal decomposition (up to 1200 °C) increases from 9.3429(6) to 9.3715(7) Å, whereas the parameter *c* slightly decreases from 6.8912(7) to 6.8854(7) Å. The lattice parameters of the final product of the thermal decomposition are close to fluorapatite, containing only traces of hydroxyl groups in the crystal structure.[41] In addition, in the FT-IR spectra the bands corresponding to carbonate and gelatine were not observed anymore. Thus, the final product after thermal decomposition (up to 1200 °C) is fluorapatite without gelatine and carbonate ions.

Morphology and Morphogenesis. Two different kinds of morphologies of the composite aggregates are found in the different Liesegang bands: so-called fan–like as well as fractal aggregates, which were already described for the case of noncarbonated fluorapatite−gelatine nanocomposites.[15−24] The fractal growth mechanism[15] dominates in the P and MP bands, whereas the fan–like growth mechanism[22] preferentially occurs in the MC and C bands. In the M band, both types of morphologies and also some intermediate forms are

(40) Tônsuaadua, K.; Peldb, M.; Leskeläa, T.; Mannonenc, R.; Niinistöa, L.; Veidermab, M. *Thermochim. Acta* **1995**, *256*, 55.
(41) Rodriguez-Lorenzo, L. M.; Hart, J. N.; Gross, K. A. *J. Phys. Chem. B* **2003**, *107*, 8316.

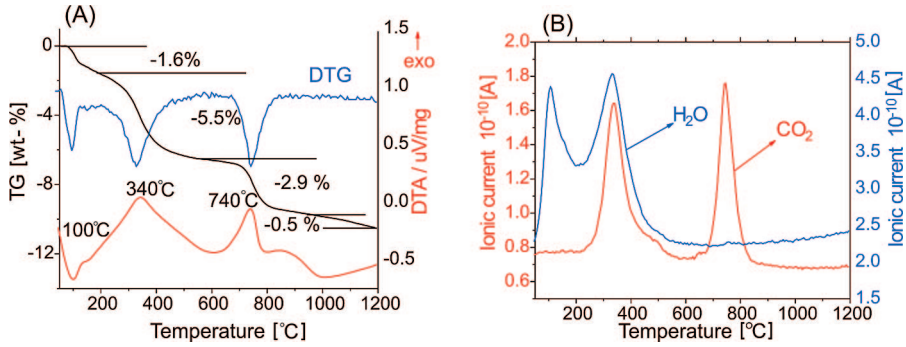

Figure 8. (A) Relative mass loss $\Delta m/m$ (TG), its first derivative (DTG), and the DTA of carbonated fluorapatite−gelatine composites with contents of carbonate and gelatine of 5.8 and 2.3 wt %, respectively; (B) mass spectroscopic (MS) diagram of the gas phases (H_2O and CO_2) released from the composite with increasing temperature.

Table 3. Thermal Decomposition of the Biomimetic Carbonated Fluorapatite Gelatine Composite (contents of carbonate and gelatine of 5.8 and 2.3 wt %, respectively)

temperature range	processes	mass loss (wt %)
room temperature to 200 °C	release of adsorbed water	1.6
200−600 °C	partial decomposition of gelatine release of constitutional water from the channels of the apatite crystal structure transformation of $[HPO_4]^{2-}$ groups to phosphate and pyrophosphate partial removal of carbonate from the apatite component	5.5
600−1200 °C	final pyrolysis of residual organics complete removal of carbonate from the apatite component	3.4

found. In previous investigations, it was shown by molecular dynamics simulations[22] that the preimpregnation of gelatine by calcium ions causes stiffening and rigidity of the triple-helical protein molecules, whereas preimpregnation by phosphate ions keeps the gelatine macromolecules flexible. It was also pointed out that the fan–like and the fractal growth series may be characterized in terms of more "crystallographic" (straight, hard) and more "biological" (bent, soft), respectively. Figure 9 shows the SEM images illustrating the changes of dumbbell shaped morphologies of carbonated fluorapatite−gelatine nanocomposites with increasing content of carbonate ions in the fractal and the fan−like growth series. The morphogenesis of our model system is in general accordance with the growth processes of pure fluorapatite-gelatine nanocomposites with a central "free bridge" for the fractal series (blue arrows in Figure 9) and a central growth plane for the fan-like series (red arrows in Figure 9), respectively. However, the carbonated composite aggregates are clearly more rounded and compressed and exhibit significant tendencies to form peanutlike morphologies with increasing carbonate content. Selected stages of the fractal morphogenesis (SEM images) of carbonated fluorapatite gelatine nanocomposites with contents of carbonate and gelatine of ∼3 and 2.4 wt %, respectively, are shown in Figure 10. This (fractal) morphogenesis of the biomimetic composite is starting with an elongated rounded seed developing via dumbbell states to finally just-closed (notched) spherical aggregates. The complete aggregate morphogenesis from elongated seeds to spheres takes approximately one week. However the nucleation and growth processes within the gelatine plugs occur accidentally overtime (due to local variations of the pH, ion-concentration, etc.) and therefore after 21 days, all types of aggregates are still present. Further supporting evidence for the composite nature of the grown aggregates is illustrated in Figure 11, where light microscopic images of completely dissolved particles in EDTA solution (0.25 M, pH 5) are presented. The images show that after complete dissolution of the apatite component an exact copy of the original morphology remains in form of a gelatine residue (jellyfish-like specimens).

Figure 12A shows the SIM image of an initial dumbbell stage of the carbonated fluorapatite gelatine nanocomposite with a carbonate content of ∼ 4 wt % and belonging to the fractal growth series with the characteristic (central) "free bridge". Compared with the pure fluorapatite−gelatine nanocomposite the carbonated specimen reveals a more compressed and rounded habit. The inner structures of the carbonated and the pure fluorapatite gelatine nanocomposites (Figure 12B−D) in this early state of the fractal form development (morphogenesis) are related in a way that bent patterns in both systems extend from the central areas in direction of the outer boundaries (faces). By this, the formation of face steps is indicated at opposite ends of the specimen. In the case of the noncarbonated fluorapatite−gelatine nanocomposite, the end-faces were already identified as the basal planes (001) of the hexagonal apatite system[22] and the bent patterns (Figure 12D) correspond to the extension of gelatine fibrils, which follow the intrinsic electrical dipole field of the composite system.[24] The structuring of the carbonated composite (Figure 10C), however, is more filigree and not as distinct (sharp) as that observed for the noncarbonated specimen (Figure 12D). Furthermore, the carbonated system reveals indications for a core−shell arrangement as indicated by the white-spot regions around the central core. The described changes in structure and morphology may be due to different sizes of the nanosubunits which form and develop the composites on the meso−macroscale.[23]

To determine the influence of carbonate on the size of the nanosubunits of the carbonated fluorapatite, we used TEM and XRD. Figure 13 shows the TEM images of enlarged parts of thin cuts of spherical aggregates of biomimetic fluorapatite and carbonated fluorapatite (car-

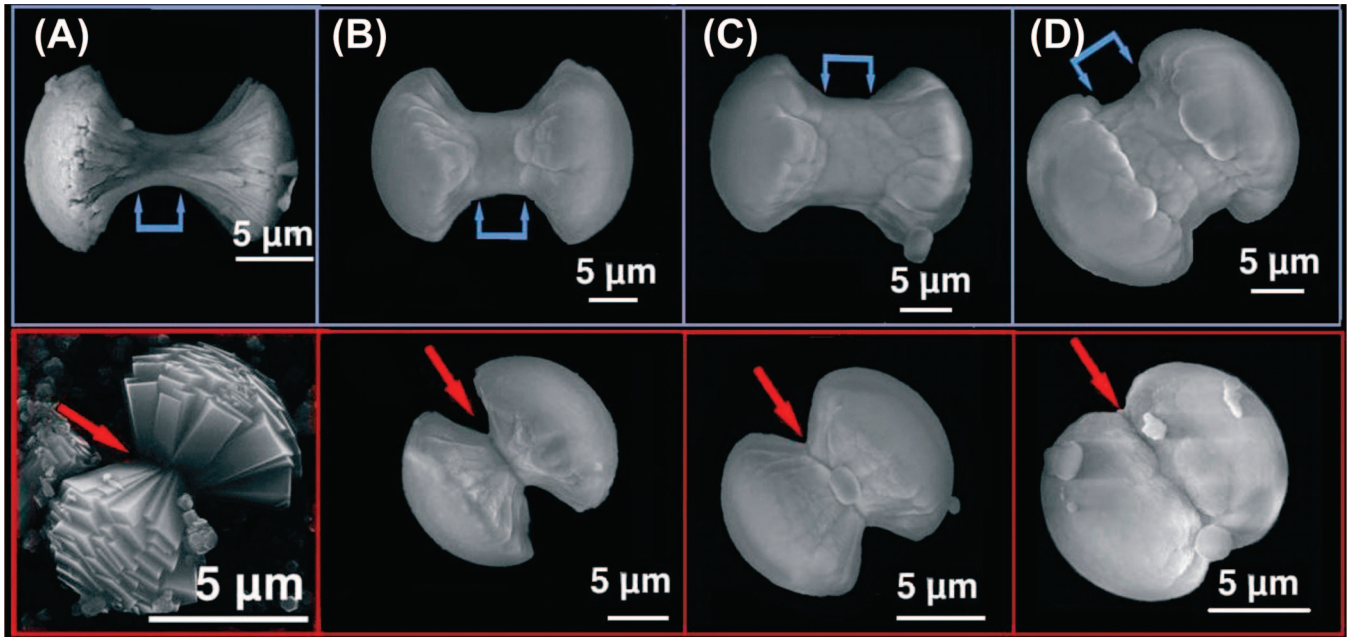

Figure 9. SEM images illustrating the changes of dumbbell-shaped morphologies of carbonated fluorapatite−gelatine nanocomposites with increasing contents of carbonate for the fractal (top row) and the fanlike (bottom row) growth series. The blue and red arrows indicate the specific characteristics for the two different morphological developments: a central "free-bridge" for the fractal series and a central growth plane for the fanlike series, respectively. Carbonate contents: (A) ~0,[21,22] (B) ~2, (C) ~ 3, and (D) ~6 wt %.

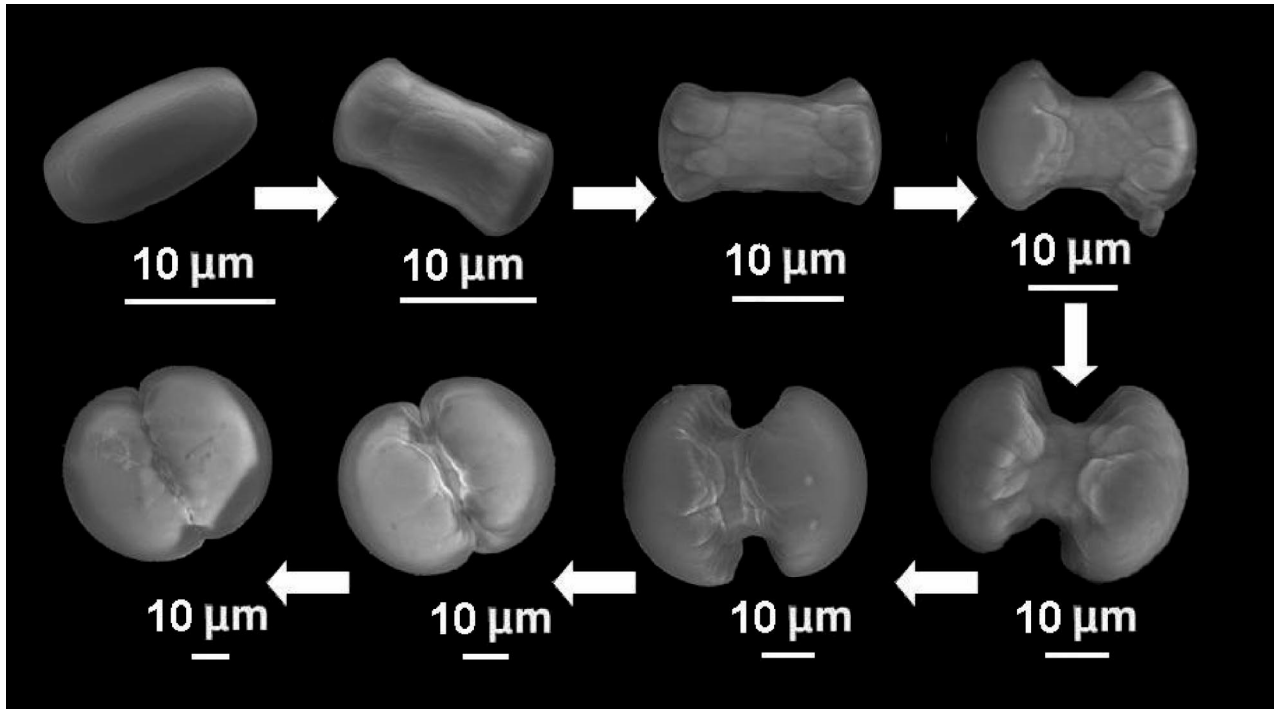

Figure 10. Selected sequence of SEM images of developing states of the self-assembled fractal growth of carbonated fluorapatite−gelatine composite aggregates with a content of carbonate about 3 wt %: from an elongated (rounded) seed via dumbbell shapes to finally just-closed spheres.

bonate content ~ 4 wt %) composites. In agreement with our previous observations,[17,18] the biomimetic fluorapatite composite is composed of small elongated subunits with preferred crystallographic orientation along [001]. The length of the subunits is about several hundred nanometers. In contrast, the carbonated composite aggregates contain nanosubunits that are significantly smaller (less than 100 nm in length). The results of the TEM investigations are confirmed by the calculations of the coherence lengths of the nanodomains along their *c*- and *a*-axes from the Scherrer equation. The results show that for samples with carbonate contents from 0.06 to 4 wt % (obtained from the M-Liesegang bands) the coherence length along [001] decreases from approximately 300 to 70 nm (Figure 14). In contrast, the coherence length along [100] is almost the same in both systems and amounts to approximately 30 nm. This trend in coherence lengths was also observed by LeGeros for carbonated hydroxyapatite.[42] Thus, it can be concluded that the change in morphology of the carbonated aggregates may be due to the less anisotropic

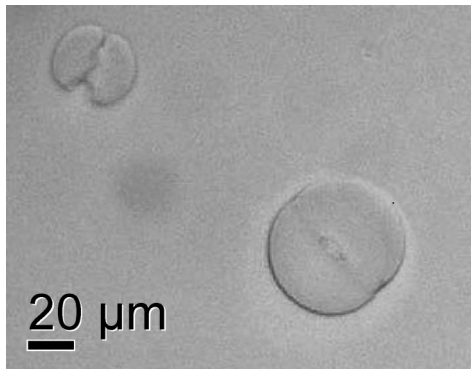

Figure 11. Light-microscopic image of the gelatine residues of completely dissolved carbonated fluorapatite−gelatine composite aggregates (dumbbell and just-closed sphere) in EDTA solution (0.25 M, pH 5). For further details, see the text.

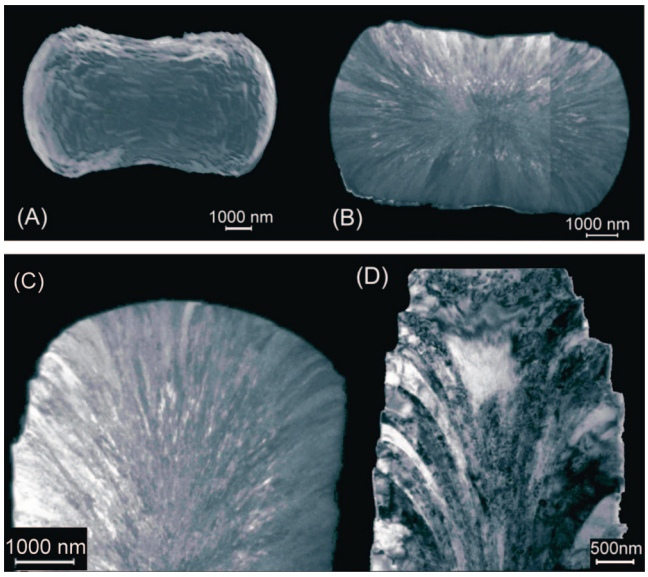

Figure 12. (A) Scanning ion image of a composite seed (early growth state, fractal growth mechanism) of carbonated fluorapatite−gelatine composite with a carbonate content of about 4 wt %; (B) overview (TEM micrograph) of a longitudinal FIB thin cut of the composite seed (A); (C) zoomed area of the TEM image (B); (D) TEM image of a FIB thin cut of a "mature" seed of the fluorapatite−gelatine composite.[21,22,24] For further details, see the text.

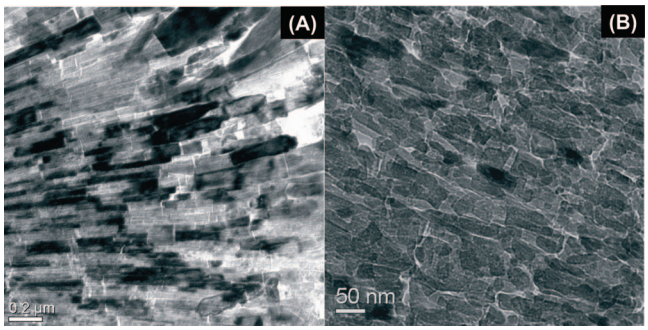

Figure 13. TEM images (ultra thin slices) of zoomed areas within fractal grown aggregates of fluorapatite−gelatine composites with different carbonate content, indicating differences in nanostructuring of the composites. Carbonate contents: (A) ∼0, and (B) ∼4 wt %. For further details, see the text.

(less elongated) habit of the carbonated fluorapatite nanosubunits compared with the more elongated nanosubunits of the pure fluorapatite composite.

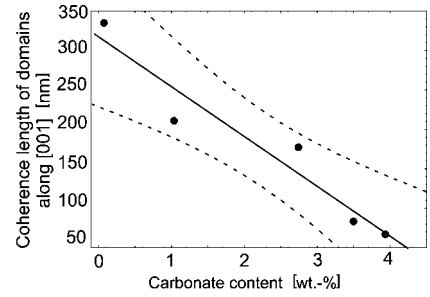

Figure 14. Variation in the coherence length of nanosubunits along [001] of the carbonated fluorapatite composite with different carbonate contents. The dashed lines indicate the 95% confidence interval for the regression curve. For further details, see the text.

Conclusion

Morphogenesis and structure of noncarbonated fluorapatite-gelatine nanocomposites have already been studied in detail in previous investigations.[15−24] The present work is a further step toward the natural composite system and is focused on the biomimetic synthesis of carbonated fluorapatite−gelatine nanocomposites. By this, the level of complexity of the chemical system under consideration is significantly increased and bears strong resemblance to the biosystem (carbonated hydroxyapatite-protein/collagen) which plays a decisive role in the human body as functional material in the form of bone and teeth.

The carbonated fluorapatite−gelatine composites with variable carbonate content on the phosphate position in the fluorapatite crystal structure (so-called B-type substitution) were synthesized by the double diffusion technique within a gelatine gel. By means of chemical analyses, FT-IR and Raman spectroscopy, XRD, and TG/DTA/MS analyses, it was shown that the aggregates grown within the Liesegang bands represent inorganic−organic nanocomposites. The gelatine content in the biomimetic composite corresponds to about 2−3 wt %. On the basis of our analytical data, the general empirical formula of the carbonated fluorapatite-gelatine composites (obtained from the M-Liesegang band) is given as follows

$$(Ca_xNa_y\square_{10-(x+y)})\{[PO_4]_{n-z}[CO_3]_k[HPO_4]_z\}\times \{F_m[OH]_s, (\square, H_2O)_{2-(s+m)}\}p\ \text{Gelatine(wt \%)} \quad (5)$$

where $x = 8.75-9.77$; $y = 0.24-0.49$; $n = 4.80-5.99$; $k = 0.01-1.20$; $z = 0.99-0.22$; $m = 2-1.73$; $s < 0.2$; $p = 2-3$; $(x + y) \leq 10$; $(m + s) \leq 2$; $(n + k) = 6$; $z = (12 + n + s + m - 2x - y)$.

Besides the "built-in" carbonate, hydrogenphosphate, and sodium, ions we also determined a Ca deficiency as well as a deficiency of $F^-(OH^-)$ ions, which is typical for biological apatite. In addition, the content of carbonate, sodium, and the organic component is close to that of dental enamel. The composite nature of the grown aggregates was demonstrated by chemical analysis as well as by decalcification experiments.

Concerning the morphology of carbonated fluorapatite-gelatine composite aggregates, the observations can be summarized by a phenomenological sequence along habit-

(42) LeGeros, R. Z.; Trautz, O. R.; LeGeros, J. P.; Klein, E.; Shirra, W. P. *Science* **1967**, *155*, 1409.

changes of the individuals with varying carbonate content. Two kinds of morphogeneses are observed: the so-called fan–like and the fractal series, which in general were already described for pure fluorapatite−gelatine nanocomposites.[15−24] The morphogenesis starts with an elongated (rounded) seed and develops via dumbbell states to closed spherical aggregates. The shapes of carbonated composite aggregates are significantly rounded and compressed. They exhibit a tendency to form peanutlike morphologies with increasing carbonate content. It is also demonstrated that the incorporation of carbonate into the composite causes dramatic effects with respect to the size of the nanosubunits composing the mesoscopic and macroscopic aggregates. The coherence length of the nanosubunits along [001] decreases from approximately 300 to 70 nm with increasing carbonate content in the composites from 0.06 to 4 wt %. In contrast, the coherence length of the nanodomains along [100] is almost independent of the carbonate content and amounts to approximately 30 nm. Thus, we assume that the change of the morphology of the aggregates may be due to the less anisotropic (less elongated) habit of the carbonated fluorapatite nanosubunits compared with the more elongated nanosubunits of the pure fluorapatite composite. Further investigations are needed in order to clarify the growth process in general, as well as the nature of the composite interactions in more detail.

Acknowledgment. The authors gratefully acknowledge the Fonds der Chemischen Industrie for generous support. We also thank the following staff members of the Max-Planck-Institut für Chemische Physik fester Stoffe for experimental support and fruitful discussions: Dr. Raul Cardoso, Dr. Yurii Prots, Dr. Horst Borrmann, Dr. Gudrun Auffermann, Dr. Stefan Hoffmann, and Susann Müller, as well as Hannelore Dallmann (TU Dresden).

CM8005748